Quantum Electronics **50** (10) 962–966 (2020)

https://doi.org/10.1070/QEL17378

Acousto-optic modulators for fibre-optic lines

V.M. Epikhin, P.V. Karnaushkin

Abstract. **The specific features of efficient matching of acousto-optic devices with single-mode fibres for the cases of isotropic and anisotropic diffraction are considered. The acousto-optic interaction geometry, optimal for modulating an arbitrarily polarised light beam with a possibility of tuning its frequency shift in the range up to ~10 MHz, is chosen. Acousto-optic modulators/frequency shifters based on paratellurite (TeO_2), pigtailed with polarisation-maintaining and non-polarisation-maintaining fibres, have been developed for wavelengths of 1064 and 1550 nm, and their main technical parameters are investigated.**

Keywords: *acousto-optic modulators/frequency shifters, single-mode fibres, optical loss, modulation contrast, polarisation contrast, rise time, working bandwidth.*

1. Introduction

The urgency of acousto-optic (AO) devices incorporated into fibre-optic lines (FOLs) is related to the advantages of closed optical channels: high degree of physical and information protection against external impacts, reliability and stability of parameters in the absence of mechanical displacements, high operating speed, flexible arrangement of small-size optical units in complex schemes, and possibility of switching optical signals in fibre communication lines [1]. Modulators/frequency shifters with a fibre output can be used to design small-size transportable optical and microwave frequency standards [2–4].

Necessary conditions for designing fibre AO devices with low optical loss are careful matching of FOLs, microlenses and acousto-optic cell (AOC), as well as their precise mounting, alignment, and fixation. These operations need special equipment and additional labor expenditures, as a result of which the device cost increases. In addition, their design imposes principal limitations on some important technical characteristics.

The purpose of this work was to design fibre-pigtailed acousto-optic modulators/frequency shifters (FPAOM/FS) with single-mode fibres and study experimentally their parameters.

V.M. Epikhin All-Russian Scientific Research Institute of Physical-Technical and Radiotechnical Measurements (VNIIFTRI), 141570 Mendeleevo, Moscow region, Russia; e-mail: epikvm@mail.ru;
P.V. Karnaushkin Perm State University, ul. Bukireva 15, 614990 Perm, Russia; e-mail: KarnaushkinPV@pnppk.ru

Received 2 June 2020; revision received 21 July 2020
Kvantovaya Elektronika **50** (10) 962–966 (2020)
Translated by Yu.P. Sin'kov

2. Specific features of FPAOM/FSs limiting their functionality

Let us consider the specific features of FPAOM/FS with an AOC based on single-crystal paratellurite (TeO_2), a material possessing a unique combination of acoustic, optical, and acousto-optic properties [5] and making it possible to implement efficient diffraction of both isotropic and anisotropic types.

Figure 1 shows a schematic of FPAOM/FS, where the optical axes of light beams are denoted by straight lines. Since identical fibre-optical cables (FOCs) are attached to both sides of FPAOM/FS, the optical loss at diffracted beam introduction into an FOC will be minimum in two cases: (i) a collimated light beam is used (the Rayleigh length of Gaussian beam greatly exceeds the distance between collimators C1 and C2 [6]), collimators are applied in stationary frequency shifters, and no requirement are imposed on the FPAOM/FS operating speed and (ii) a convergent light beam is focused at the centre of the sound column (whose length is on the order of Rayleigh beam length), focusers are installed instead of collimators, and the beam intensity can be rapidly modulated.

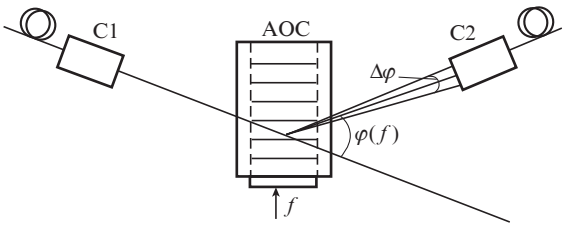

Figure 1. FPAOM/FS optical scheme.

In the former case the requirements to the alignment of FPAOM/FS elements are less stringent, because the optical loss is noncritical to the distance from the collimators to the AOC; therefore, we used the scheme with collimated beams in our modulators.

Limitation of the FPAOM/FS working bandwidth. A specific feature of the developed FPAOM/FSs is the presence of a receiving microlens with a narrow angular field, beyond

which the losses of diffracted light beam introduced into an FOC sharply increase. It can easily be shown [7, 8] that the following expression is valid for diffraction of arbitrary type:

$$\Delta\varphi \approx \frac{\lambda\Delta f}{V}, \tag{1}$$

where $\Delta\varphi$ is the change in the angle between the wave vectors of zero and first diffraction order in air with a change in frequency Δf, λ is the radiation wavelength in vacuum, and V is the ultrasonic-wave (USW) phase velocity. The angular field of collimator C2 is $\beta = D/A$ (D is the fibre core diameter, A is the distance from the centre of the collimator lens to the fibre end face). For a collimated beam, A is approximately equal to the collimator focal length F. Since $\Delta\varphi = \beta$, the FPAOM/FS reception frequency band caused by the angular drift of diffracted beam is

$$\Delta f_r \approx \frac{DV}{\lambda F}. \tag{2}$$

At the extreme points of this band, the centres of the circles imaging the end face of the FOC core with a diameter D and the beam waist with a diameter $2w \approx D$ are spaced by a distance of w. One can easily see that the relative overlap of the areas of the corresponding circles is $0.39 \approx -4$ dB in this case. It follows from (2) that the frequency band Δf_r for isotropic diffraction from a longitudinal USW in TeO_2 is much wider than for anisotropic diffraction from a transverse USW, because the ratio of their longitudinal (V_{lg}) and shear (V_s) velocities varies from 5 to 7 [5].

As was shown in [4], to solve problems calling for maximally wide working bandwidth with the use of collimated beams in TeO_2, the optimal way is to apply a longitudinal wave with a wave vector oriented along the Z axis of the crystal. In this case, $V_{lg} = 4260$ m s^{-1}, which is close to the maximum longitudinal-wave velocity in TeO_2 (4600 m s^{-1}). The uniqueness of this AO interaction geometry is as follows: When the diffraction efficiency is close to unity, it barely depends on the radiation polarisation. In addition, orthogonally polarised diffracted beams propagate at the AOC output parallel to each other and, therefore, have identical optical losses at the FOC input.

When using a shear operating USW (as applied to FPAOM/FS), the specific features of anisotropic diffraction in TeO_2 are significant (by almost an order of magnitude) narrowing of the reception band Δf_r, radical (by more than an order of magnitude) increase in the acousto-optic figure of merit M_2, and the necessity of applying only plane-polarised radiation.

With allowance for this specificity, we used isotropic diffraction from a longitudinal USW with a wave vector oriented parallel to the Z axis of TeO_2 crystal in the developed FPAOM/FSs.

The frequency band characteristics of a real AO device include also the matching band Δf_m of piezoelectric transducer (PET) [7] and the width of AOC frequency apparatus function Δf_{af} [9, 10]. According to estimates and experimental data, for the chosen AOC geometry at $f > 50$ MHz [4], $\Delta f_r \ll \Delta f_m \approx \Delta f_{af}$; the two latter parameters amount to several tens of MHz. Thus, the working bandwidth Δf of the developed FPAOM/FS is determined by the above-described geometric factor: $\Delta f = \Delta f_r$.

The band Δf_r can be significantly widened using a more complex double-crystal FPAOM/FS, consisting of two identical AOCs rotated by 180° [11]. In this case, the angular frequency drift of collimated light beam after the first AOC is compensated for in the second AOC. In sum, the angular displacement $\Delta\varphi$ is transformed into a parallel displacement Δl of the optical axis of output beam before the output collimator.

The width of the Δf_r band can also be increased using the scheme of FPAOM/FS with convergent beams; in this case, the light beam is focused at the centre of the sound column, and the beam waist image is formed on the end face of the output fibre core. Since simple estimates are hindered in this situation, experimental studies must be performed.

Limitation of FPAOM/FS operating speed. According to [12], the diffraction efficiency of a Gaussian light beam from a USW emitted by a homogeneous, limited in space converter, depend on the coefficient a: the ratio of the light beam divergence ψ_{lgt} (at the level of $1/e^2$) and the sound beam divergence ψ_{snd} (at the level of about -4 dB) in the diffraction plane,

$$a = \frac{\psi_{lgt}}{\psi_{snd}}. \tag{3}$$

Substituting $\psi_{lgt} = 4\lambda/(\pi n 2w)$ and $\psi_{snd} = V/(Lf)$, where n is the refractive index of TeO_2 and L is the PET length (in the light propagation direction) into (3), and assuming that $2w = H/k$, where H is the PET width and $k > 1$ is the 'margin' coefficient for facilitating alignment, we obtain

$$a = \frac{4k\lambda fL}{\pi nVH}. \tag{4}$$

Furthermore, we perform estimation using the formula for acoustic power density ρ, which is necessary for gaining the maximum diffraction efficiency of plane wave, $T = 1$ [7]:

$$\frac{\pi}{\lambda}\left(\frac{\rho L^2 M_2}{2}\right)^{1/2} = \frac{\pi}{2}. \tag{5}$$

Then we arrive at

$$a = \frac{4kf\lambda^2}{\pi nHV(2\rho M_2)^{1/2}}. \tag{6}$$

We apply also the formula for the rise (switching) time of diffracted light pulse at the intensity level of 0.1–0.9 [7]:

$$\tau = 0.64\frac{2w}{V} = 0.64\frac{H}{kV}. \tag{7}$$

With allowance for (6),

$$\tau = \frac{0.58f\lambda^2}{anV^2(\rho M_2)^{1/2}}. \tag{8}$$

As one would expect, the k value does not affect τ, whereas the power necessary for obtaining the acoustic power density ρ is proportional to k. Formulas (7) and (8) are correct provided that $f \geqslant 1/\tau$, which yields the necessary slope of the acoustic pulse leading edge. To estimate τ_{min}, we assume that $f \approx 1/\tau_{min}$. Finally, we have

$$\tau_{\min} \approx \frac{0.76\lambda}{V(an)^{1/2}(\rho_p M_1)^{1/4}}, \quad (9)$$

where ρ_p is the maximum (threshold) acoustic power density. In the pulsed regime, at a constant time-averaged threshold density $\langle\rho_{imp}\rangle = \rho_p$, the peak pulsed density ρ_{imp} increases by a factor of m: $\rho_{imp} = m\rho_p$, where m is the on–off time ratio of the pulsed sequence. In this case the averaging time should be shorter than the settling time of AOM stationary thermal regime, which is estimated to be several hundreds of microseconds under these conditions. It is important that specifically the average density determines the PET overheating and thermal degradation.

The maximum value of pulsed density ρ_{imp} is limited by the PET electrical breakdown. Here, the following relation holds true:

$$\rho_{imp} = \frac{U_{br}^2}{RLH}, \quad (10)$$

where U_{br} is the electrical breakdown voltage and R is the PET active resistance.

The following experimental value of the threshold acoustic power density without PET degradation was obtained in [4] for the continuous regime of the RF signal: $\rho_p \approx 2 \times 10^6$ W m^{-2} (L = 2.5 mm, H = 0.2 mm, $R \approx 5$ Ω). The PET in use had a form of a two-side polished lithium niobate ($LiNbO_3$) plate (Y + 36° cut) attached to the TeO_2 crystal. As the experience of dealing with such PETs shows, their breakdown voltage is several tens of volts. We assume for definiteness that $U_{br} \approx 30$ V. Substituting these parameters into formula (10), we find that $\rho_{imp} \approx 360 \times 10^6$ W m^{-2}. Note that this density is obtained under quite realistic conditions: the mean acoustic power $\langle P\rangle$ = 1 W and m = 180.

The τ_{min} value was estimated with the following parameters: a = 1 (maximum diffraction efficiency $T_{max} \approx 0.8$ [12]), $M_2 \approx 30 \times 10^5$ s^3 kg^{-1} [5], $n \approx 2.2$ [5], and $\rho_{imp} \approx 360 \times 10^6$ W m^{-2}. Substituting these values into (9), we obtain the lower estimates for the FPAOM/FS rise time: τ_{min}(1064 nm) ≈ 2 ns and τ_{min}(1550 nm) ≈ 3 ns. As follows from (5) and (8), smaller τ_{min} values at a constant density ρ_p can be implemented only by reducing T_{max}, which limits the range of practical applications.

The aforementioned minimum values of the rise time can be obtained provided that all other frequency band characteristics of FPAOM/FS (Δf_m, Δf_{af}, Δf_r) are not limited by the value of $\sim 0.5/\tau_{min}$ [13]. In the opposite case, the real rise time τ_{real} can be estimated from the following formula: $\tau_{real} \approx 0.5/\Delta f_{min}$, where Δf_{min} is the smallest one among the aforementioned band characteristics.

3. FPAOM/FS design

FPAOM/FS parameters. Isotropic diffraction from a longitudinal USW propagating along the Z axis was used in both fabricated FPAOM/FS versions. The design parameters for both versions are listed in Table 1. Here, P_{max} is the RF signal power necessary to achieve the maximum diffraction efficiency T_{max} and Q is the Klein–Cook parameter, which determines the diffraction regime [14]. The calculated values of the reception band Δf_r^{calc} (at the level of –4 dB) for collimators with F = 4.2 mm are also presented. Note that Δf_r can be doubled using commercial collimators with a minimum focal length of 2 mm [15].

An FPAOM/FS consists of a housing measuring 122 × 33 × 13.5 mm, which contains an AOC; a device for matching PET and RF channel impedances (50 Ω); and several aspherical lens collimators with fibre-optical cables, terminating with FC/APC optical connectors. An RF connector of SMA type is mounted on the housing to supply control signals.

Collimators with a lens diameter of 2.5 mm and a non-polarisation-maintaining single-mode fibre were mounted on the FPAOM/FS Photon-6200, and collimators with a lens diameter of 8 mm and polarisation-maintaining Panda-type fibre for measuring the maximally attainable polarisation contrast were installed on Photon-6201.

Optical alignment of FPAOM/FS units. The collimators were aligned with an AOC using a hardware/software complex (HSC), including vibration-isolation base; precise positioner with six degrees of freedom; auxiliary positioner; light source with working wavelengths of 635, 1081, and 1539.0 nm; optical power meter; generator; and personal computer. The HSC schematic is shown in Fig. 2.

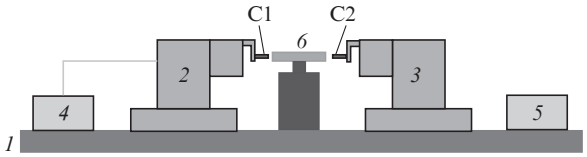

Figure 2. Schematic of the HSC for FPAOM/FS alignment: (*1*) vibration-isolation base; (*2*) precise positioner with six degrees of freedom; (*3*) auxiliary positioned; (*4*) light source; (*5*) optical power meter; (*6*) FPAOM/FS.

The characteristics of the precise positioner are as follows: the step over the X, Y, and Z axes is 0.1 μm and the step over the angular axes θ_x, θ_y, and θ_z is 3.6″.

The optical alignment included the following stages: preparation, preliminary alignment, final alignment, and fixation. In the preparation stage, the AOC (rigidly connected to the housing) was fixed on the table, and collimators C1 and C2 were fixed in pneumatic holders, rigidly connected to the positioners. The FPAOM/FS was connected to the generator, and C1 and C2 were connected to the light source and optical power meter, respectively. During the preliminary alignment collimators C1 and C2 were tuned

Table 1. FPAOM/FS design parameters.

FPAOM/FS	Wavelength λ/nm	Polarisation	Aperture H/mm	Centre frequency f/MHz	φ/deg	a	$Q/4\pi$	T_{max}	P_{max}/W	Δf_r^{calc}/MHz
Photon-6200	1064	arbitrary	1.2	70	1.02	0.36	2.2	0.93	1.4	5.7
Photon-6201	1550	plane	1.1	75	1.59	0.53	3.2	0.90	2.7	5.6

Table 2. FPAOM/FS experimental parameters.

FPAOM/FS	Wavelength λ/nm	Total optical loss σ/dB	Modulation contrast K/dB	Polarisation contrast K_{pol}/dB	Rise time τ/ns	RF signal power P_{max}/W	Centre frequency f/MHz	Working bandwidth Δf_r^{exp}/MHz
Photon-6200	1064 ± 50	–1.9	–68	–	112	1.4	70	6.5
Photon-6201	1550 ± 60	–1.8	–56	–27	112	2.9	75	6.5

(relative to the AOC) to the maximum transmitted beam intensity, and an RF signal was applied to the FPAOM/FS. The alignment was performed first at a wavelength of 635 nm and then at the FPAOM/FS working wavelengths. During the final alignment the diffracted beam transmitted through the optical system was sought for. Then the positions of collimators C1 and C2 along linear and angular axes were corrected to obtain a maximum diffracted beam intensity. In the stage of connection fixation, collimators C1 and C2 were glued with spacers (previously mounted in the housing). A low-shrinkage epoxy glue was used; it was polymerised using 365-nm radiation of a UV LED with a focusing lens. Then the holders of collimators C1 and C2 were removed.

To estimate the quality of optical alignment of collimators, we performed a preliminary alignment (without fixing units) and measured passive optical loss with RF signal switched-off in the configurations C1 → AOC → C2 and C1 → air gap → C2 (with air gap of the same thickness as the AOC). The measured losses, including the loss on two optical outlets, in the version with an air gap and in the presence of AOC were found to be 2.3 and 3.5 dB, respectively, for Photon-6200 and 1.0 and 1.4 dB, respectively, for Photon-6201.

4. Experimental study of FPAOM/FS

The experimental parameters of the developed and fabricated FPAOM/FSs are listed in Table 2. The spectral ranges in which the reflectance of antireflection coating is below 0.2% are indicated for both radiation wavelengths.

The radiation sources were lasers LCS-T-12 (1064 nm) and LP1550-SAD2 (1550 nm), and a power meter PM20C with an input optical connector FC/PS(APC) was used to detect laser radiation. The RF signal source was a G4-107 generator with a power amplifier ZHL-1-2WX+. The RF signal frequency was controlled by an electron frequency meter Ch3-63. The laser sources were connected with the power meter using 1-m segments of P3-980A-FC-1 and P3-1550PM-FC-1 FOCs.

The total optical losses were calculated from the formula $\sigma = 10\lg(I_{max}^{+1}/I_0)$, where I_{max}^{+1} is the maximum photoresponse in the +1st diffraction order and I_0 is the photoresponse for a laser connected with the power meter through a FOC. The modulation contrast K was calculated from the formula $K = 10\lg(I_{P=0}^{+1}/I_{max}^{+1})$, where $I_{P=0}^{+1}$ is the photoresponse in the +1st diffraction order in the absence of an RF signal ($P = 0$), and the polarisation contrast was calculated from the formula $K_{pol} = 10\lg(I_{\perp}^{+1}/I_{max}^{+1})$, where $I_{\perp}^{+1}$ is the maximum photoresponse in the +1st diffraction order for radiation polarised orthogonally to the incident beam polarisation. The rise time is $\tau = 0.64(2w/V_{lg})$.

Note that the total optical loss for Photon-6200 turned out to be smaller than the previously measured passive loss, which can be explained by more careful final alignment. The larger modulation contrast for Photon-6200 (as compared with Photon-6201) is likely due to the smaller external diameter of the collimator lens and more efficient spatial selection of zero- and first-order beams. The measured bandwidth values Δf_r^{exp} exceed the corresponding calculated values Δf_r^{calc}, which can be explained by the increase in the actual diameter of light beam waist on the end face of receiving FOC (correspondingly, $2w > D$) due to the nonideality of FPAOM/FS optical system.

As follows from [16], the parameters of the FPAOM/FSs developed by us are comparable with those of the corresponding analogues from leading manufacturers.

5. Conclusions

(1) The specific features and limitations arising when matching AO devices with single-mode fibres in the cases of isotropic and anisotropic diffraction in TeO_2 were considered. Estimation formulas were derived, and the frequency bandwidth and minimum rise time were estimated for the FPAOM/FS.

(2) The acousto-optic interaction geometry, optimal for modulating the intensity and frequency of an arbitrarily polarised light beam with a working bandwidth of ~10 MHz was chosen.

(3) FPAOM/FSs Photon-6200 and Photon-6201, pigtailed to polarisation-maintaining (λ = 1550 nm) and non-polarisation-maintaining (λ = 1064 nm) optical cables, were fabricated.

(4) The main technical parameters were determined for FPAOM/FSs: diffraction efficiency, working band, control power, optical loss, rise time, modulation contrast, polarisation contrast.

(5) The parameters of the developed FPAOM/FSs are as good as those of the analogues from leading manufacturers of fibre-pigtailed AO devices.

References

1. Antonov S.N. *J. Tech. Phys.*, **64**, 242 (2019) [*Zh. Tekh. Fiz.*, **89**, 274 (2019)].
2. Berdasov O.I., Gribov A.Yu., Strelkin S.A., Slyusarev S.N. *Al'm. Sovrem. Metrol.*, (11), 81 (2017).
3. Kupalov D.S., Baryshev V.N., Blinov I.Yu., Boiko A.I., Domnin Yu.S., Kopylov L.N., Kupalova L.N., Novoselov A.V., Khromov M.N. *Al'm. Sovrem. Metrol.*, (11), 95 (2017).
4. Epikhin V.M., Baryshev V.N., Slyusarev S.N., Aprelev A.V., Blinov I.Yu. *Quantum Electron*, **49**, 857 (2019) [*Kvantovaya Elektron.*, **49**, 857 (2019)].
5. Blistanov A.A., Bondarenko V.S., Perelomova N.V., Shaskol'skaya M.P. *Akusticheskie kristally* (Acoustic Crystals) (Moscow: Nauka, 1982) p. 242.
6. Eichler J., Eichler H.J. *Laser: Bauformen, Strahlfuhrung, Anwendungen* (Berlin: Springer, 2006; Moscow: Tekhnosfera, 2012).
7. Magdich L.N., Molchanov V.Ya. *Acoustooptic Devices and Their Applications* (New York: Gordon and Breach, 1989; Moscow: Sov. Radio, 1978).
8. Epikhin V.M. *Opt. Spectrosc.*, **119**, 273 (2015) [*Opt. Spektrosk.*, **119**, 287 (2015)].

9. Balakshy V.I., Parygin V.N., Chirkov L.E. *Fizicheskie osnovy akustooptiki* (Physical Principles of Acousto-Optics) (Moscow: Radio i Svyaz', 1985) p. 119.
10. Gazalet M.G., Waxin G., Rouvaen J.M., Torguet R., Bridoux E. *Appl. Opt*., **23**, 674 (1984).
11. Mazur M.M., Mazur L.I., Shorin V.N., Ryabinin A.V. RF Patent No. RU 2703930 (priority date 22 October, 2019).
12. Maydan D. *IEEE J.*, **QE-6** (1), 15 (1970).
13. Dieulesaint E., Royer D. *Elastic Waves in Solids. Applications to Signal Processing* (New York: Wiley, 1980; Moscow: Nauka, 1982).
14. Klein W.R., Cook D.D. *IEEE Trans*., **SU-14** (3), 123 (1967).
15. www.thorlabs.com.
16. www.isomet.com; www.brimrose.com; www.gandh.com.